A dualband bandpass filter with tunable bandwidths for automotive radar and 5G millimeter-wave applications

Thierno Amadou Mouctar Balde[1], Franklin Manene[2], Franck Moukanda Mbango[3,4]
[1]Department of Electrical Engineering, Pan African University Institute for Basic Sciences, and Technology and Innovation, Nairobi, Kenya
[2]Department of Electrical and Control Engineering, Egerton University, Nakuru, Kenya
[3]Electrical and Electronics Engineering Laboratory, Marien Ngouabi University, Brazzaville, Congo
[4]Faculty of Sciences and Techniques, Marien Ngouabi University, Brazzaville, Congo

Article Info

ABSTRACT

A compact dual wideband bandpass filter for automotive radar (AR) and 5G millimeter-wave (mmWave) applications with adjustable bandwidths is presented in this work. The filter is based on microstrip dual-mode edge-coupled stub-loaded resonators (SLR). The novelty of this configuration is that it allows independent control of the bandwidths which is not obvious for many reported SLR-based filters. To achieve an overall size of $1.23\lambda\_g \times 2.02\lambda\_g$, these resonators are coupled and bent into U-shape, T-shape, and E-shape. The U-shaped resonator, based on a quarter-wavelength transmission line, is coupled to the T-shaped element which constitutes the main feed line to obtain the dual-band response. Having a symmetrical structure, the design is studied using the even-odd mode analysis. The layout is made using the Ansys high-frequency structural simulator (HFSS) and fabricated on Rogers RO3010 with a thickness of 1.28 mm, a dielectric constant of 10.2, and a loss tangent of 0.0022. The measured bandwidths are 660 MHz and 880 MHz at central frequencies of 23.92 GHz and 28.38 GHz respectively. The measured insertion losses are less than 3.9 dB and the return losses are greater than 17 dB in both bands. A good agreement is obtained between simulated and experimental results.

Corresponding Author:

Thierno Amadou Mouctar Balde
Department of Electrical Engineering,
Pan African University Institute for Basic Sciences and Technology and Innovation
Nairobi, Kenya
Email: thierno.mouctar@students.jkuat.ac.ke

1. INTRODUCTION

The millimeter-wave (mmWave) spectrum is nowadays considered the best-promising frequency band for the next generation of wireless communication systems [1]. This is due to the enormous bandwidth and high data rate it offers [2]. On the other hand, the development of autonomous driving systems and the rising of government policies for vehicle safety have led to considerable growth of automotive radar technologies in recent years [3]–[7]. Hence, bandpass filter (BPFs) will significantly impact the overall system performance [8]–[10], and the multiband function is preferred since applications are evolving daily [11]–[13]. However, these filters should be compact to ease their integration with other radiofrequency (RF) components, highly selective, deep transmission zeros around the passbands, and low insertion loss [11]. Several techniques and methods have been investigated throughout the literature to design high-frequency multiband BPFs [14], among them, multi-mode resonators. A dual-band filter is designed in [15] using stub-loaded multiple mode

resonators for 5G mid-band applications. Likewise, two coupled open-loop resonators loaded with stubs, spiral resonators, and lumped capacitors are utilized to offer a dual-band behavior in reference [11]. A filter based on folded dual-mode quarter-wave resonators, presented in [16], allows obtaining a three-band response for global system for mobile communications (GSM), global positioning system (GPS), and wireless fidelity (Wi-Fi) applications. Although these filters achieve good performance, using vias leads to a complex manufacturing process. A mmWave single band BPF based on coupled line and center-tapped upper and lower stepped impedance resonators (SIR) is presented in [17], however, the overall circuit size is quite big. Altaf *et al.* [18], a dual-mode ring resonator with two folded half-wavelength stepped impedance resonator (SIR) is used to design two mmWave single bands BPFs for 34 GHz and 40 GHz, respectively. Furthermore, a non-resonating U-shape node is studied and combined with two dual-mode open-loop resonators to design a dual-band BPF for 5G mmWave applications [12]. Similarly, a Conventional microstrip line structure is used to design a millimeter-wave BPF operating at 28 GHz [19]. Nevertheless, some of these filters are bulky in size, others have a poor return loss, and more importantly, tunable bandwidths or independent control of the passbands was only achieved in [16].

More advanced techniques, such as substrate integrated waveguide (SIW), low-temperature cofired ceramic (LTCC), and complementary metal-oxide-semiconductor (CMOS) or Gallium Arsenic (GaAs) were respectively used in [10], [20]–[22] to design mmWave BPFs. These approaches have advantages such as miniaturization, selectivity improvement, and insertion loss mitigation, however, the fabrication cost and complexity are among their major weaknesses. Therefore, considering mmWave applications' filtering requirements such as circuit size and ease of integration with less complexity, microstrip filters appear to be the best options for 5G mmWave applications [13], [23]–[26]. Consequently, a compact wideband dual-band BPF based on microstrip single layer reduction (SLR) is presented in this paper for augmented reality (AR) at 24 GHz and 5G mmWave at 28 GHz. This filter is analyzed using the even-odd mode approach because of its symmetrical structure. However, the novelties of the proposed filter are the independent tuning of the bandwidths which is demonstrated in the sections ahead and its simple and compact design. To validate the design approach, the filter was printed on Rogers 3,010 substrate material and measured. A good agreement between simulated and experimental results was observed. The remaining part of this work is structured as shown in; Section 2 focuses on the mathematical modeling, and section 3 highlights the design concept while in Section 4 the results are analyzed and interpreted.

2. MATHEMATICAL MODELING

The proposed filter is designed by folding dual-mode SLRs. An SLR is typically made of a transmission line with uniform impedance and an open or short-circuited stub (Figure 1). Here, a quarter-wavelength ($\lambda/4$) transmission line is employed to design a U-shaped SLR whose lengths are calculated at 24 GHz, which provides the desired bandwidths. Therefore, the elements of the filter can be analyzed through the input impedance of a microstrip transmission line [14] given as (1). Considering the symmetrical structure of the filter, input impedances can be expressed through the even-odd mode method which simplifies and reduces the analysis to half [27].

$$Z_{in} = Z_0 \frac{Z_L + jZ_o \tan(\theta)}{Z_0 + jZ_L \tan(\theta)} \quad (1)$$

where $\theta = \beta L$ is the electrical length of the line, L its physical length, and β the phase constant, given by (2):

$$\beta = 2\pi f_r \frac{\sqrt{\varepsilon_{eff}}}{c} \quad (2)$$

where c represents the speed of light in the free space, f_r the resonant frequency, and ε_{eff} is the dielectric constant given by (3):

$$\varepsilon_{eff} = \frac{\varepsilon_r + 1}{2} + \frac{\varepsilon_r - 1}{2}\left(1 + 12\frac{h}{2}\right)^{-\frac{1}{2}} \quad (3)$$

where ε_r is the substrate relative permittivity, w is the width of the line, and h is the dielectric thickness. The basic structure of an SLR is given in Figure 1(a), and its even and odd mode configuration in Figure 1(b) and Figure 1(c) respectively [14]. Based on (1), the even input impedance of the SLR, which corresponds to an open circuit, ($Z_L = 0$) can be expressed as (4).

$$Z_{in,(e)} = -jZ_2 \frac{Z_2 \tan\theta_1 \tan\theta_2 - Z_1}{Z_1 \tan\theta_2 + Z_2 \tan\theta_1} \tag{4}$$

Similarly, the odd input impedance which is equivalent to a short circuit ($Z_L = \infty$) is calculated using (3).

$$Z_{in,(o)} = jZ_1 \tan\theta_1 \tag{5}$$
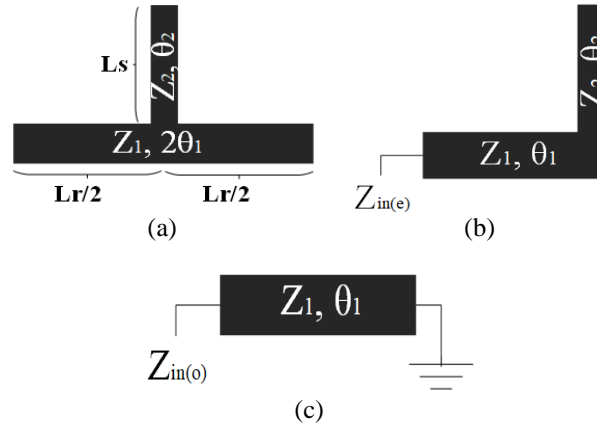
Figure 1. Stub-loaded resonator configurations in (a) topology of a basic SLR, (b) even mode configuration, and (c) odd mode configuration

The resonance condition of the even mode is $1/Z_{in,(e)} = 0$ and that of the odd mode is $1/Z_{in,(o)} = 0$. Therefore, this approach is applied to all the elements shown in Figure 2 to obtain their input impedances expressed in terms of characteristic impedances (Z_0) and electrical lengths (θ). As the T-shaped resonator (Figure 2(a-b)) is equivalent to the basic SLR topology presented in Figure 1, the mathematical expressions remain the same. However, the corresponding even and odd input impedances of the inverted U-shaped element (Figure 2(c-d)) is given as (6) and (7), and that of the middle U-shaped resonator (Figure 2(e-f)) by (8) and (9), and finally for the E-shaped resonator (Figure 2(g-h)) by (10) and (12). It is important to mention that the resonant frequencies are obtained by combining the resonance condition and the phase constant equation of the quasi-TEM mode behavior of the microstrip line [15].

$$Z_{in_{(e)}}^{(\cap)} = jZ_4 \frac{\tan\theta_4 \tan\theta_5 - K_4}{\tan\theta_5 + K_4 \tan\theta_4} \tag{6}$$

$$Z_{in_{(o)}}^{(\cap)} = jZ_4 \tan\theta_4 \tag{7}$$

$$Z_{in_{(e)}}^{(U)} = jZ_6 \frac{\tan\theta_6 \tan\theta_7 - K_6}{\tan\theta_7 + K_6 \tan\theta_6} \tag{8}$$

$$Z_{in_{(o)}} = jZ_6 \tan\theta_6 \tag{9}$$

$$Z_{in_{(e)}}^{(E)} = Z_8 \frac{Z_L + jZ_8 \tan\theta_8}{Z_8 + jZ_L \tan\theta_8} \tag{10}$$

$$Z_L = jZ_9 \frac{\tan\theta_9 \tan\theta_{10} - K_9}{1 + K_9 \tan\theta_9} \tag{11}$$

$$Z_{in_{(o)}}^{(E)} = jZ_8 \frac{\tan\theta_8 + K_8 \tan\theta_9}{1 - K_8 \tan\theta_8 \tan\theta_9} \tag{12}$$

where $K_4 = \frac{Z_5}{Z_4}, K_6 = \frac{Z_7}{Z_6}, K_8 = \frac{Z_9}{Z_8}$ and between $K_9 = \frac{Z_{10}}{Z_9}$ are impedance ratios between Z_5 and Z_4, Z_7 and Z_6, Z_9 and Z_8, Z_{10} and Z_9 while $\theta_4 = \beta L_4$, $\theta_5 = \beta L_{5/2}$, $\theta_6 = \beta L_6$, $\theta_7 = \beta L_{7/2}, \theta_8 = \beta L_8$, $\theta_9 = \beta L_{9/2}$ and $\theta_{10} = \beta L_{10}$ are electrical lengths of the corresponding stubs.
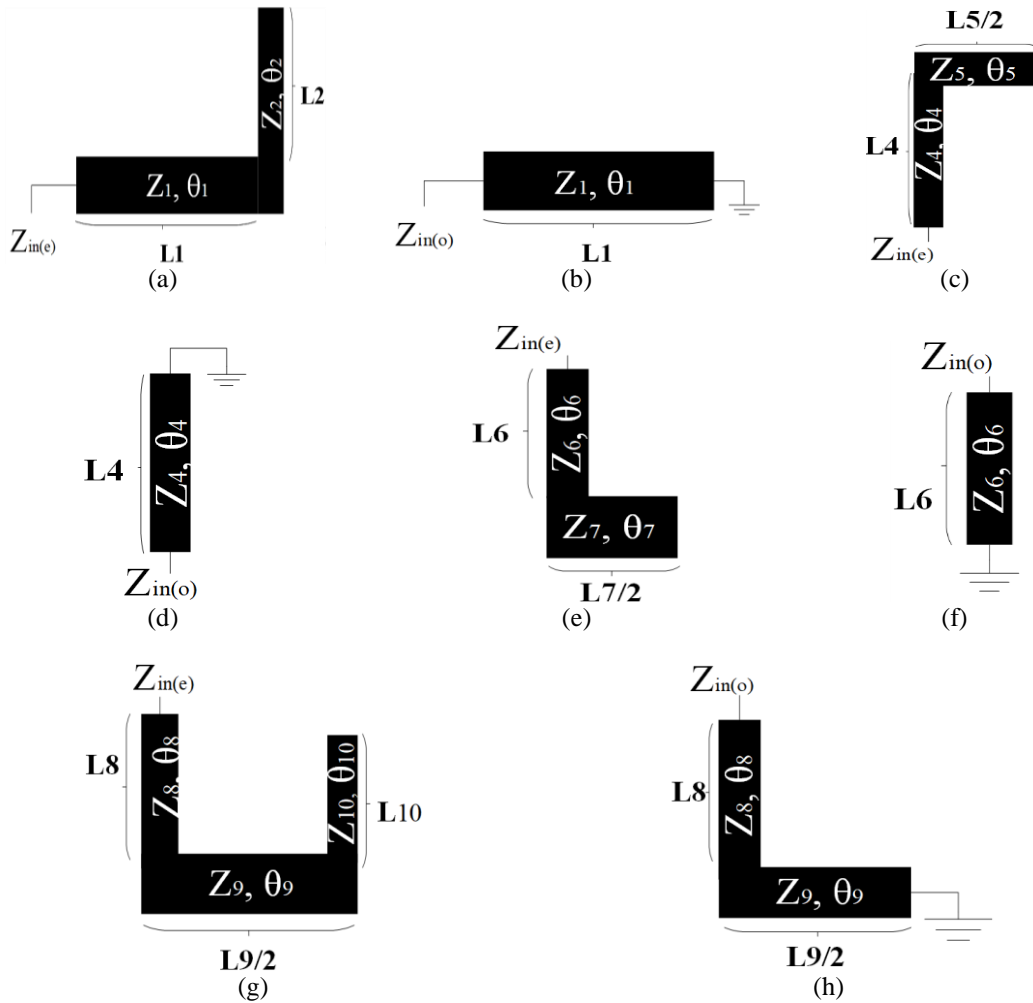
Figure 2. Even and odd mode configurations of the filter building blocks based on (a-b) T-shaped, (c-d), Inverted U-shaped, (e-f) middle U-shaped, and (g-h) E-shaped resonators.

3. FILTER DESIGN

The design simulations (Figure 3) were carried out using Ansys high-frequency structural simulator (HFSS) and the layout was printed on a $1.23\lambda_g \times 2.02\lambda_g$ Rogers RO3010 substrate material with a thickness of 1.28 mm, dielectric constant $\varepsilon_r = 10.2$, and loss tangent $tan\delta = 0.0022$ where λ_g is the guided wavelength at the center frequency (26 GHz). This configuration provides a multimode behavior that gives multiple resonant frequencies which can be independently controlled [14]. To obtain the desired dual-band response, a U-shaped quarter-wavelength resonator is placed at the center of the structure and edge-coupled with the L-shaped resonator, which acts here as the main feedline. However, each of these two resonators exhibits a dual-mode behavior, which resulted in a quad-band response as shown in Figure 3(a). To suppress undesired harmonics, a small stub of length L_3 is, firstly attached to the L-shaped, which becomes a quasi T-shaped resonator. Consequently, the band located around 30 GHz is eliminated (Figure 3(b)). Second, an inverted U-shaped element is weakly coupled with the circuit which not only eliminates the band located around 20 GHz but provides wide bands at desired frequencies 24 and 28 GHz (Figure 3(c)). Table 1 summarizes the optimum dimensions of the filter elements.

Finally, to improve the insertion loss and to deepen the transmission zeros (TZ) which represent frequencies where perfect attenuation occurs, thus improving the selectivity of the Filter, an E-shaped resonator is added in Figure 3(d) and a parasitic element is attached to the mainline to obtain the final structure show as in Figure 3(e).

(a)

(b)

(c)

(d)

(e)
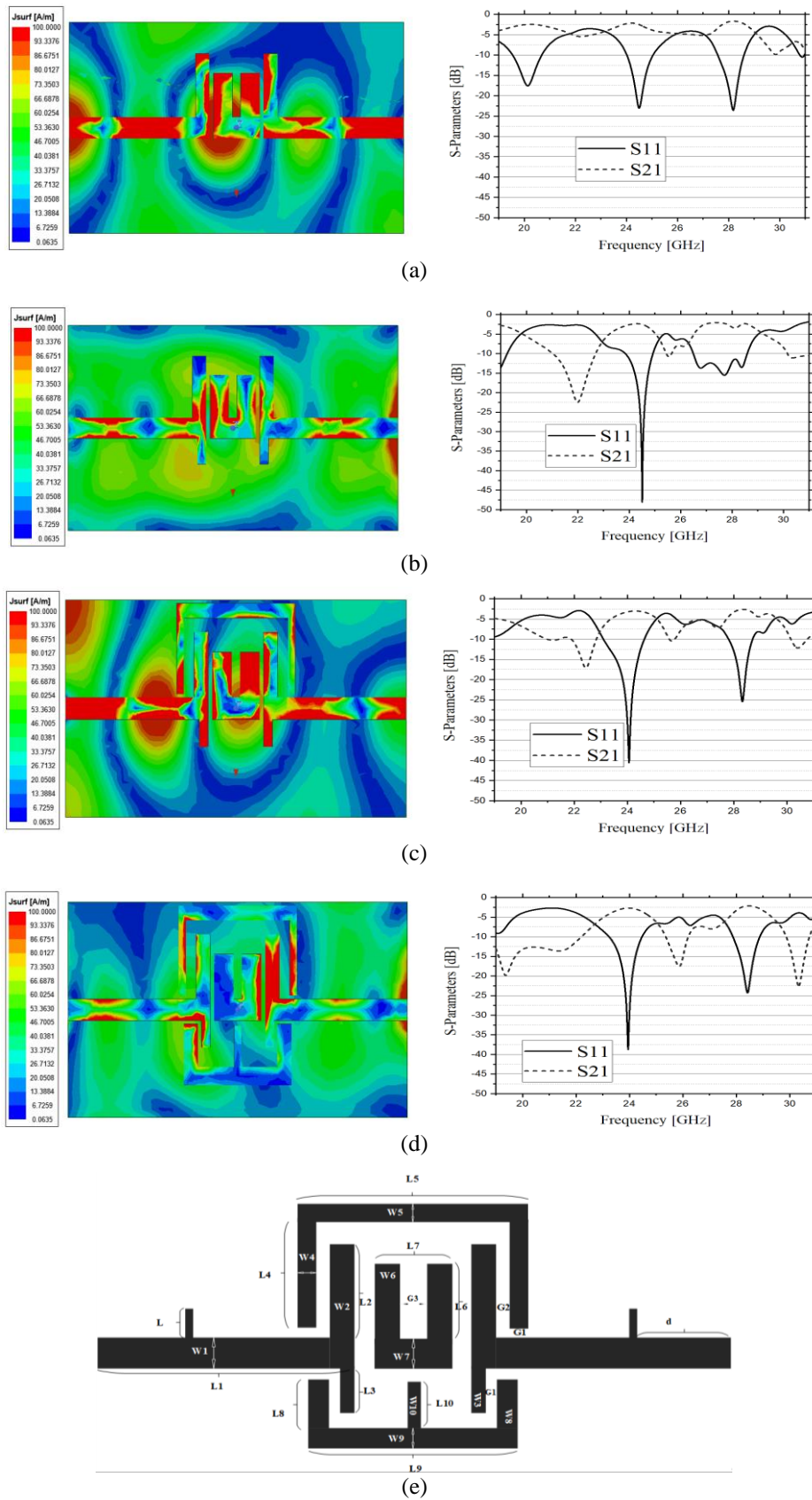
Figure 3. The proposed filter design process that yields the optimum configuration in (a) U-shaped coupled with the feedline, (b) L_3 stub is added, (c) adding the inverted U-shaped resonator, and (d) coupled E-shaped resonator, and (e) final topology of the proposed dual-band BPF

Table 1. Dimensions (mm) of the proposed dual-band bandpass filter

Parameter	Value	Parameter	Value	Parameter	Value
L1	4.1	W1	0.6	L10	1.15
L2	1.8	W2	0.4	W10	0.2
L3	0.75	W3	0.25	L	0.65
L4	2.1	W4	0.2	D	1.5
L5	3.4	W5	0.4	G1	0.1
L6	1.25	W6	0.55	G2	0.3
L7	1.35	W7	0.6	G3	0.25
L8	1.2	W8	0.4		
L9	3.1	W9	0.5		

4. RESULTS AND DISCUSSION

A compact dual-band BPF based on folded SLRs with tunable bandwidths is designed and fabricated in this paper. Two resonators T-shaped and U-shaped (Figure 2(a-e)) are employed to obtain the targeted frequency bands, while the two others inverted U-shaped and E-shaped (Figure 2(c-g)) are used for harmonics suppression and performance improvement. However, the advantage of this structure is that the bandwidths can be independently controlled (Figure 4). It has been found that the lower bandwidth can be tuned by adjusting the value of G_2 while the upper bandwidth is fixed, hence the gap between L_2 and L_4 as shown in Figure 4(a). This band may be adjusted from 23.14 GHz to 23.48 GHz on the lower side and from 24.45 GHz to 24.53 GHz in the upper part of the bandwidth reading at 10 dB of the return loss. Likewise, the second bandwidth can be tuned from 27.90 GHz to 28.18 GHz of its lower part and from 28.95 GHz to 29.80 GHz of its upper part by adjusting the length of the stub L_3 as shown in Figure 4(b). This proves that the proposed filter has the capability of independent control of the passbands. Furthermore, to validate the prototype made with the 3D electromagnetic (EM) simulator Ansys HFSS, the filter was printed on Rogers RO3010 having a thickness of 1.28 mm, a dielectric constant of 10.2, and a loss tangent equal to 0.0022, and measured using a Rohde and Schwarz ZVA50 vector network analyzer (VNA).

The simulated and measured results of the proposed filter are shown in Figure 5. A good agreement can be observed between the two with slight changes in terms of insertion loss and bandwidth. This is because of the fabrication errors and the losses introduced by SMA connectors. However, the simulated insertion losses are 1.94 dB and 2.74 dB in the lower and upper bands against 3.87 dB and 3.64 dB of the measured results at center frequencies 23.92 GHz and 28.38 GHz respectively. The measured return losses are better than 17 dB while the simulated reflection coefficients are greater than 19 dB at both bands. On the other hand, a large bandwidth greater than 1 GHz is obtained throughout the simulations while 660 MHz of bandwidth is measured in the lower band covering the short-range radar (SRR) application, and 880 MHz of bandwidth is obtained in the upper band for 5G mmWave application. Additionally, three simulated TZs are respectively generated at 19.24GHz, 25.88 GHz, and 30.43 GHz. However, only two deep TZs are obtained through the measurements.
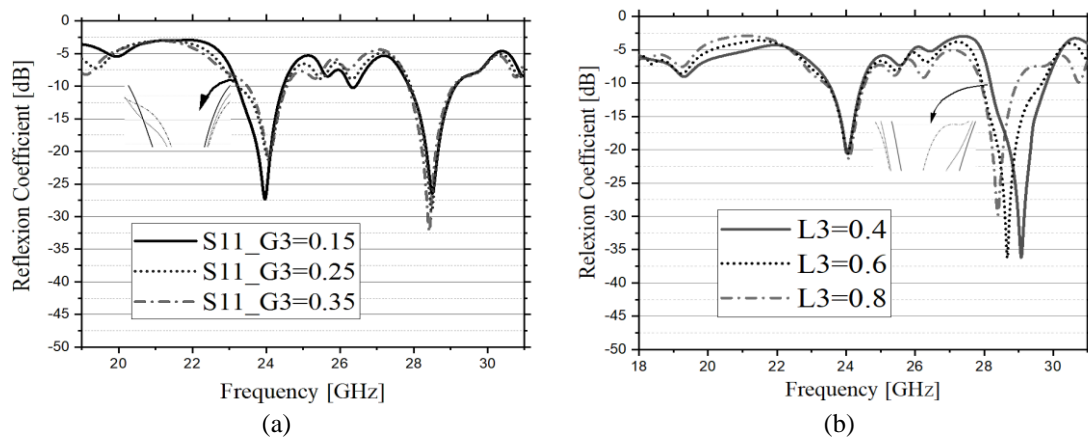
Figure 4. Process of tuning the Dualband filter bandwidths, in (a) lower band tuning by adjusting G2 and (b) the upper band tuning by varying L3

The third measured TZ located at 28.87 GHz is not as deep as its equivalent obtained via simulation. This difference can be caused by the losses and mismatches of connectors and the prototype, and also the high

loss sensitivity of mmWave circuits. The performance of this filter with similar works is presented in Table 2. It can be observed that the proposed dual-band bandpass filter achieves a good trade-off between size and loss.
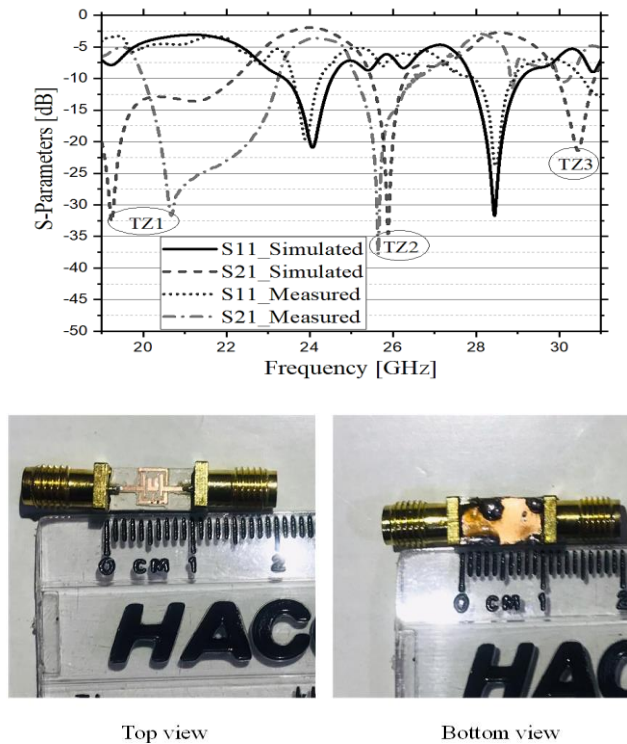
Figure 5. Simulated and measured transmission and reflection coefficient with the printed prototype

Table 2. Performance comparison with similarly published works

Ref	Freq. (GHz)	IL (dB)	RL (dB)	Technique	Size (mm2)
Lin et al. [19]	28	4	10	Microstrip	$3.28\lambda_g \times 3.53\lambda_g$
Keinicke et al. [28]	36.5	3.44	8	Microstrip	N/A
Haraz et al. [29]	14.5/28.2	1.9/4.7	13.5	Microstrip	$0.44\lambda_g \times 1.41\lambda_g$
Yeh et al. [30]	35	4.5	12	CPW on CMOS	0.225×0.55
[This work]	23.92/28.38	3.87/3.64	17.2/19.15	Microstrip	$1.23\lambda_g \times 2.02\lambda_g$

5.   CONCLUSION

In this paper, a compact wideband dual-band (23.92/28.38 GHz) bandpass filter with tunable bandwidths has been presented for automotive radar and 5G mmWave wireless applications. The dual-band response was realized by employing a $\lambda/4$ U-shaped resonator coupled with a T-shaped element acting as the principal feedline. To improve the performance of the filter and to suppress undesired harmonics, an inverted U-shaped and an E-shaped resonator were added. The simulations were carried out using Ansys HFSS and the prototype with an overall size of 58.8 mm^2 was fabricated on Rogers RO3010 having a thickness of 1.28 mm, a dielectric constant of 10.2, and a loss tangent of 0.0022. The measured insertion losses are less than 3.9 dB at both center frequencies and the return losses are better than 17 dB. The measured bandwidths are respectively 660 MHz and 880 MHz. Finally, TZs were generated which improve the roll-off skirts and the stopbands performance of the filter. The proposed BPF has many advantages such as wide and tunable bandwidths, low loss, and compact size. Its compactness eases its integration with other RF front-end components which makes it a great candidate for automotive radar and 5G mmWave applications.

REFERENCES

[1]   S. Ghosh and D. Sen, "An inclusive survey on array antenna design for millimeter-wave communications," *IEEE Access*, vol. 7, pp. 83137–83161, 2019, doi: 10.1109/ACCESS.2019.2924805.

[2]   G. Chittimoju and U. D. Yalavarthi, "A comprehensive review on millimeter waves applications and antennas," *J. Phys. Conf. Ser.*, vol. 1804, no. 1, 2021, doi: 10.1088/1742-6596/1804/1/012205.

[3]   J. Choi *et al.*, "Combining millimeter-wave radar and communication paradigms for automotive applications: A signal processing approach," May, pp. 25, 2016.

[4]   Z. Szalay, P. Varga, D. Ficzere, V. Tihanyi, F. Magyar, and G. Soós, "5G-enabled autonomous driving demonstration with a V2X scenario-in-the-loop approach," *Sensors (Switzerland)*, vol. 20, no. 24, pp. 1–24, 2020, doi: 10.3390/s20247344.

[5]   E. Gambi, G. Ciattaglia, and A. D. E. Santis, "Automotive radar application for structural health monitoring," vol. 189, pp. 79–89, 2019, doi: 10.2495/SAFE190081.

[6]   I. Bilik, O. Longman, S. Villeval, and J. Tabrikian, "The rise of radar for autonomous vehicles: signal processing solutions and future research directions," *IEEE Signal Process. Mag.*, vol. 36, no. 5, pp. 20–31, 2019, doi: 10.1109/MSP.2019.2926573.

[7]   R. Yadav, P. K. Dahiya, and R. Mishra, "Comparative analysis of automotive radar sensor for collision detection and warning system," *Int. J. Inf. Technol.*, vol. 12, no. 1, pp. 289–294, 2020, doi: 10.1007/s41870-018-0167-3.

[8]   S. Dey, S. K. Koul, A. K. Poddar, and U. L. Rohde, "Frequency and bandwidth tunable reliable MEMS bandpass filter for 24 GHz radar applications," *Int. J. RF Microw. Comput. Eng.*, vol. 31, no. 6, pp. 1–14, 2021, doi: 10.1002/mmce.22662.

[9]   B. Adli, R. Mardiati, and Y. Y. Maulana, "Design of microstrip hairpin bandpass filter for X-Band radar navigation," *Proceeding 2018 4th Int. Conf. Wirel. Telemat. ICWT 2018*, pp. 1–6, 2018, doi: 10.1109/ICWT.2018.8527781.

[10] Z. A. Bhat, J. A. Sheikh, S. D. Khan, I. Bashir, and R. Rehman, "A compact and reconfigurable dual-mode configuration substrate integrated waveguide dual-band bandpass filter for 5G and millimeter-wave communications," *Prog. Electromagn. Res. Lett.*, vol. 99, no. August, pp. 93–101, 2021, doi: 10.2528/PIERL21032602.

[11] A. A. Ibrahim, W. A. E. Ali, and M. A. Abdelghany, "Design of dual-band dual-mode band-pass filter utilizing 0 ∘ feed structure and lumped capacitors for WLAN/WiMAX applications," *Electron.*, vol. 9, no. 10, pp. 1–14, 2020, doi: 10.3390/electronics9101697.

[12] L. Shi and J. Gao, "Multitransmission zero dual-band bandpass filter using nonresonating node for 5G millimetre-wave application," *Act. Passiv. Electron. Components*, vol. 2018, 2018, doi: 10.1155/2018/7628598.

[13] A. Lalbakhsh *et al.*, "A compact C-band bandpass filter with an adjustable dual-band suitable for satellite communication systems," *Electron.*, vol. 9, no. 7, pp. 1–17, 2020, doi: 10.3390/electronics9071088.

[14] V. C. Bengin, *Advances in Multiband Microstrip Filters*, First. Cambridge, United Kingdom Cambridge: Cambridge University Press, 2015.

[15] F. M. Alnahwi, Y. I. A. Al-Yasir, A. A. Abdulhameed, A. S. Abdullah, and R. A. Abd-Alhameed, "A low-cost microwave filter with improved passband and stopband characteristics using stub loaded multiple mode resonator for 5G mid-band applications," *Electron.*, vol. 10, no. 4, pp. 1–15, 2021, doi: 10.3390/electronics10040450.

[16] A. Basit, M. I. Khattak, A. R. Sebak, A. B. Qazi, and A. A. Telba, "Design of a compact microstrip triple independently controlled pass bands filter for GSM, GPS and WiFi applications," *IEEE Access*, vol. 8, pp. 77156–77163, 2020, doi: 10.1109/ACCESS.2020.2989377.

[17] Z. A. Bhat, J. A. Sheikh, S. D. Khan, R. Rehman, and S. Ashraf, "Compact and novel coupled line microstrip bandpass filter based on stepped impedance resonators for millimetre-wave communications," *Frequenz*, vol. 75, pp. 147–152, 2021, doi: 10.1515/freq-2020-0156.

[18] A. Altaf, C. Xi, W. Shahzad, U. Dilshad, and J. Miao, "Design of millimeter-wave microstrip BPF using dual-mode ring resonator and folded half-wavelength resonators," *Proc. 2020 17th Int. Bhurban Conf. Appl. Sci. Technol. IBCAST 2020*, pp. 653–657, 2020, doi: 10.1109/IBCAST47879.2020.9044528.

[19] Y.-C. Lin, S.-C. Lin, Y.-J. Lee, and T.-Y. Huang, "Millimeter-wave bandpass filter on printed circuit board with conventional microstrip line structure," *Int. Symp. Antennas Propag.*, pp. 1–2, 2021, doi: 10.23919/isap47258.2021.9614477.

[20] G. Shen, W. Che, W. Feng, Y. Shi, F. Xu, and Q. Xue, "Ultra-low-loss millimeter-wave LTCC bandpass filters based on flexible design of lumped and distributed circuits," *IEEE Trans. Circuits Syst. II Express Briefs*, vol. 68, no. 4, pp. 1123–1127, 2021, doi: 10.1109/TCSII.2020.3033379.

[21] G. Shen, W. Feng, W. Che, Y. Shi, and Y. Shen, "Millimeter-wave dual-band bandpass filter with large bandwidth ratio using gaas-based integrated passive device technology," *IEEE Electron Device Lett.*, vol. 42, no. 4, pp. 493–496, 2021, doi: 10.1109/LED.2021.3062862.

[22] C. S. Cabello, L. F. Herran, and E. R. Iglesias, "KA-band diplexer for 5G mmWave applications in inverted microstrip gap waveguide technology," *Electron.*, vol. 9, no. 12, pp. 1–15, 2020, doi: 10.3390/electronics9122094.

[23] M. W. Applications, "WHITEPAPER implementing high performance filters in millimeter wave applications," *microwavejournal*, pp. 1–5, 2019.

[24] P. Moukala Mpele, F. Moukanda Mbango, D. B. O. Konditi, and F. Ndagijimana, "A novel Quadband Ultra Miniaturized Planar Antenna with Metallic vias and Defected Ground Structure for Portable Devices," *Heliyon*, vol. 7, no. 3, p. e06373, 2021, doi: 10.1016/j.heliyon.2021.e06373.

[25] C. L. Bamy, F. M. Mbango, D. B. O. Konditi, and P. M. Mpele, "A compact dual-band dolly-shaped antenna with parasitic elements for automotive radar and 5G applications," *Heliyon*, vol. 7, no. 4, p. e06793, 2021, doi: 10.1016/j.heliyon.2021.e06793.

[26] S. O. Coumar, "Miniaturized DGS based multi-bandpass filters for satellite applications," *J. Ambient Intell. Humaniz. Comput.*, no. 0123456789, 2021, doi: 10.1007/s12652-021-02898-3.

[27] P. Anand K. Verma, *Introduction To Modern Planar Transmission Lines: Physical, Analytical, and Circuit Models Approach*, First. New Jersey: Wiley-IEEE Press, 2021.

[28] T. Keinicke *et al.*, "Replicability of a millimeter-wave microstrip bandpass filter using parallel coupled lines," *2018 IEEE MTT-S Lat. Am. Microw. Conf. (LAMC 2018)*, pp. 1–3, 2019, doi: 10.1109/LAMC.2018.8699012.

[29] O. M. Haraz, N. Ashraf, S. Almorqi, H. Shaman, S. A. Alshebeili, and A. R. Sebak, "Millimeter-wave microstrip diplexer using elliptical open-loop ring resonators for next-generation 5G wireless applications," *Microw. Opt. Technol. Lett.*, vol. 58, no. 1, pp. 106–110, 2016, doi: 10.1002/mop.29506.

[30] L. K. Yeh, C. Y. Chen, and H. R. Chuang, "A millimeter-wave CPW CMOS On-chip bandpass filter using conductor-backed resonators," *IEEE Electron Device Lett.*, vol. 31, no. 5, pp. 399–401, 2010, doi: 10.1109/LED.2010.2043333.

BIOGRAPHIES OF AUTHORS

Thierno Amadou Mouctar Balde ⓘ 🕾 SC Ⓟ was born in Republic of Guinea, in 1994. He received his Bachelor's degree in Electronics Engineering from Gamal Abdel Nasser University, Conakry in 2019. He is currently a graduate student in Electrical Engineering Telecommunications option at Pan African University Institute for Basic Sciences Technology and Innovation (PAUISTI), Kenya. His research interests include Microwave Circuits Design, Microstrip Technology, and 5G Millimeter-wave Filters. He can be contacted at email: thierno.mouctar@students.jkuat.ac.ke.

Dr. Franklin Manene ⓘ 🕾 SC Ⓟ is a lecturer in the Department of Electrical and Control Engineering, Egerton University Kenya, as well as a part-time lecturer at Pan African University Institute for Basic Sciences Technology and Innovation (PAUISTI), Juja (Kenya). He received his Bachelor of Technology degree in Electrical communication engineering from Moi University (Kenya) in 1999. In 2007, He obtained a Master of Science degree in Electrical engineering (Telecommunications engineering) from Jomo Kenyatta University of Agriculture and Technology. He was awarded a Ph.D. in Electrical Engineering (Electromagnetics) in 2014 from Florida Institute of Technology, USA. His research interests include microwave systems design, wireless applications, and Metamaterials. He can be contacted at email: franklin.manene@egerton.ac.ke.

Prof. Dr. Franck Moukanda Mbango ⓘ 🕾 SC Ⓟ was born in Pointe-Noire, in 1973 (Republic of Congo). He received an engineering degree in microwave electronics from Mouloud Mammeri University, Tizi-Ouzou (Algeria), in 2001. In 2003 and 2008, he received his M.Sc. degree in microwave circuits from the National Polytechnic Institute (INP) and his Ph.D. degree from the Joseph Fourier University (UJF) in optics and Radio Frequency at Grenoble (France). From 2009 to 2014, he was involved in some Telecommunication industrial projects as an R&D Engineer and Research Assistant Consultant to ALTRAN Technologies for Vallourec (Paris), also as Electromagnetic Compatibility (EMC) Engineer to Scientific and Technical Center for Building (CSTB), Grenoble. In addition, he is a former part-time Senior Lecturer at Pan African University Institute for Basic Sciences Technology and Innovation (PAUISTI), Juja (Kenya), for African Union. He is currently a CAMES Associate Professor at Marien Ngouabi University, Brazzaville (Congo). He lectured on the propagating guided waves and the advanced microwave engineering systems. His research interests include multidisciplinary physics and electronic engineering applied to the high-frequency material measurement techniques, Electromagnetic modeling of microwave devices and wireless applications, electromagnetic waves' impact on the environment, and microwave design (antennas and circuits) systems. He can be contacted at email: franck.moukandambango@umng.cg.